ChemComm

COMMUNICATION

Cite this: *Chem. Commun.*, 2018, **54**, 2365

Received 2nd January 2018,
Accepted 7th February 2018

DOI: 10.1039/c8cc00029h

rsc.li/chemcomm

In situ growth of all-inorganic perovskite nanocrystals on black phosphorus nanosheets†

Hao Huang,[a] Jia Li,*[a] Ya Yi,[a] Jiahong Wang,[a] Yihong Kang,[a] Paul K. Chu,[b] H. C. Ong[c] and Xue-Feng Yu*[a]

This communication describes a novel low-dimensional nanohybrid structure consisting of all-inorganic perovskite nanocrystals (NCs) growing *in situ* on two-dimensional (2D) black phosphorus (BP) nanosheets. Such a nanohybrid structure promises synergetic properties by combining the respective strengths of perovskite materials and BP, which opens new opportunities for next-generation optoelectronic devices.

Low-dimensional hybrid structures composed of zero-dimensional (0D) nanocrystals (NCs) or quantum dots (QDs) located on the surface of 2D materials have recently attracted extensive interest.[1] These structures can offer more degrees of freedom to design heterojunctions between various low-dimensional quantum systems. As a result, synergetic effects can be expected by combining the respective strengths of 0D and 2D materials, which opens new opportunities to realize high-performance optoelectronic devices.

A variety of low-dimensional materials have been used as building blocks to construct a 0D–2D hybrid structure. For instance, graphene[2–6] has been shown to produce strong fluorescence quenching of 0D semiconductor NCs or QDs, demonstrating enhanced ability for energy harvesting and photodetection. In addition, transition metal dichalcogenides (TMDCs), such as MoS_2,[7,8] WSe_2,[9] WS_2[10] and SnS_2,[11] have been coupled to QDs, justifying the improved performance of 2D semiconductors in light collection. In fact, the enhancement of the optoelectronic performance is mainly attributed to charge transfer (CT) and Förster energy transfer (FET) occurring at the interface of 0D and 2D materials.[3,11–15] The photo-excited FET from 0D materials (donor) to 2D materials (acceptor) generates electron–hole pairs. The transport of photogenerated carriers then causes the photocurrent (I_{ph}) in the 0D–2D system under a bias. In the process of generating photocurrent, 0D materials serve as an effective light harvester owing to the large absorption cross-section, size-tunable bandgap, and high quantum yield. At the same time, 2D materials make contributions based on their excellent electronic/electrical properties. For example, the higher carrier mobility of 2D materials leads to a larger I_{ph} under the same illumination conditions and at a fixed bias voltage.[3]

Obviously, to produce more efficient optoelectronic devices, the 0D–2D hybrid structure should possess the following merits. First of all, 2D materials should have a good balance in terms of various electronic/electrical properties. Secondly, 0D materials should have superior photon absorption, high quantum yield, and optical tunability. Thirdly, a strong bonding between 0D materials and 2D materials is necessary not only for the device stability but also for more efficient charge transfer.[16] To date, although much research has focused on hybrid structures by combining 2D graphene or TMDCs with traditional colloidal QDs, much less efforts have been made to explore hybrid structures based on 2D BP and perovskite NCs, which promise great potential both for fundamental studies and optoelectronic applications. Besides, the traditional method to construct a hybrid structure involves simply placing 0D materials on the surface of 2D materials or using linking ligands in between. In comparison, there have been few reports on direct *in situ* growth of 0D materials on 2D materials, though this strategy can provide more precise control of the distribution uniformity and loaded amount of NCs on 2D materials as well as the strong bonding between the NCs and 2D materials.

In this work, we design and construct a new 0D–2D hybrid structure consisting of perovskite NCs directly growing *in situ* on BP sheets. Benefiting from a good balance between the high carrier mobility (up to 1000 $cm^2\ V^{-1}\ s^{-1}$)[17] and satisfactory current on/off ratio (up to 10^5),[18] BP can bridge the gap between graphene and TMDCs.[18,19] In addition, perovskite NCs or QDs

[a] *Center for Biomedical Materials and Interfaces, Shenzhen Institutes of Advanced Technology, Chinese Academy of Sciences, Shenzhen 518055, People's Republic of China. E-mail: jia.li1@siat.ac.cn, xf.yu@siat.ac.cn*
[b] *Department of Physics and Department of Materials Science and Engineering, City University of Hong Kong, Tat Chee Avenue, Kowloon, Hong Kong, China*
[c] *Department of Physics, The Chinese University of Hong Kong, Shatin, Hong Kong, China*

† Electronic supplementary information (ESI) available. See DOI: 10.1039/c8cc00029h

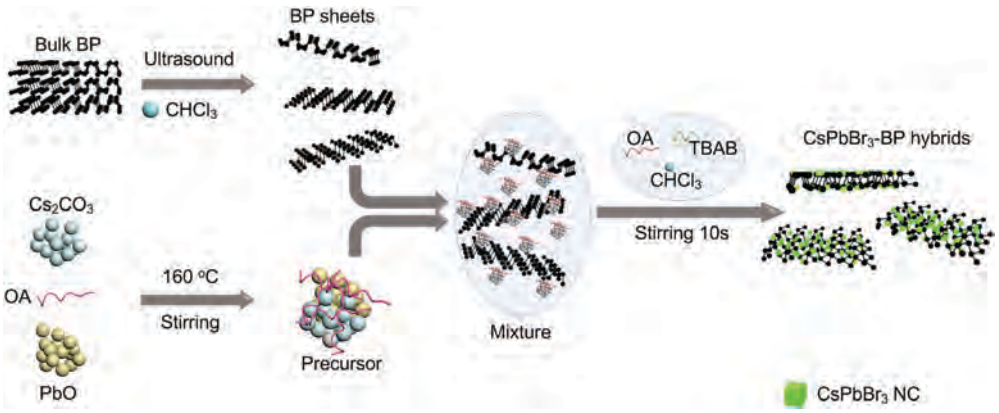

Scheme 1 Synthesis of the $CsPbBr_3$–BP hybrids.

stand out with a high quantum yield (90%),[20] efficient photon absorption and excellent optical tunability.[21,22] More importantly, the facile solution-based process for perovskite crystallization[23,24] and the reaction compatibility of BP materials provide the opportunity to synthesize perovskite NCs directly on BP sheets.

The process to synthesize the perovskite–BP hybrid is illustrated in Scheme 1. A solution-based synthesis process is used for the direct growth of inorganic $CsPbX_3$ (X = Br, I) NCs on solvent-exfoliated BP sheets at room temperature. No ligand exchange steps are required in this process and different halide elements are employed for broadband adjustment to cater to diverse optoelectronic applications. We also demonstrate the reduction of the photoluminescence (PL) lifetime from the $CsPbBr_3$–BP hybrid structure, implying the non-radiative energy transfer or electron transfer occurring in this hybrid structure.

The first step is to prepare BP nanosheets by the solvent exfoliation method. Selection of an appropriate solvent is critical for the preparation of materials. Although *N*,*N*-dimethylformamide (DMF) is an efficient exfoliation solvent used to prepare 2D layered materials, it unavoidably remains on the materials' surface after exfoliation and degrades the perovskite $CsPbX_3$ (X = Cl, Br, I).[25] Therefore, the traditional exfoliation method based on DMF is not suitable for the preparation of perovskite–BP hybrid structures. Consequently, the low-boiling solvent chloroform ($CHCl_3$) is adopted to enable effective exfoliation of BP with less influence on perovskite NCs.

The BP sheets were synthesized by a modified liquid exfoliation method.[26] The BP crystal was ground in a mortar with $CHCl_3$. The mixture was sealed and probe-sonicated for several hours. Afterwards, the solution was centrifuged for 5 min at 300 rpm and the supernatant containing micrometer-scale BP sheets was collected. Although the solution composed of BP sheets shows broadband absorption ranging from the ultraviolet to near-infrared regions, the absorption intensity, especially in the long wavelength region, is relatively low due to the small thickness of the 2D BP sheets (Fig. S1a, ESI†). The transmission electron microscopy (TEM) image shows that the as-prepared BP sheets have a lateral size of over 1 μm and the translucent appearance reveals that the BP sheets are thin (Fig. S1b, ESI†). The high-resolution transmission electron microscopy (HR-TEM) image inset in Fig. S1b (ESI†) discloses a lattice spacing of 0.25 nm, corresponding to the (111) plane of the BP crystal[27] and indicating high crystallinity. The atomic force microscopy (AFM) image and height profile curves have been shown in Fig. S2 (ESI†). One can see that the thickness of the as-prepared BP sheets ranges from 15 nm to 22 nm. After BP exfoliation, the perovskite precursor was prepared. The perovskite precursor in the form of Cs-oleic and Pb-oleic was prepared by mixing Cs_2CO_3, oleic acid (OA), and PbO at 160 °C under continuous stirring until the solution became transparent. The precursor was then diluted with $CHCl_3$. Afterwards, an appropriate amount of the diluted precursor was added to the $CHCl_3$ solution containing BP sheets and stirred for several minutes. In this step, Cs-oleic and Pb-oleic adsorbed onto the surface of BP sheets to form the perovskite precursor–BP mixture. The adsorption results from the interaction between the lone pair electrons in BP and the metal ions Cs^+/Pb^{2+}.[28] Finally, another Br-precursor consisting of $CHCl_3$, OA and tetrabutylammonium bromide (TBAB) was rapidly injected into the mixture under vigorous stirring for 10s. The solution turned yellow-green and the $CsPbBr_3$–BP hybrid was obtained. It should be noted that pure $CsPbBr_3$ QDs were formed when no BP sheets were added in the third step (Fig. S3, ESI†).

The TEM images of the synthesized $CsPbBr_3$ QDs and $CsPbBr_3$–BP hybrids are depicted in Fig. 1. The typical $CsPbBr_3$ QDs synthesized without participation of BP sheets possess a uniform cubic morphology with an average size of about 9 nm, as shown in Fig. 1a and b. The HR-TEM (Fig. 1c) image shows a lattice fringe spacing of 0.29 nm, arising from the (200) plane of the cubic phase of perovskite $CsPbBr_3$.[25] Fig. 1d–f show the TEM and HR-TEM images of the $CsPbBr_3$–BP hybrid materials. All of the hybrid samples examined by TEM, HR-TEM, and SEM were prepared by performing long and repeated centrifugation to remove perovskite NCs not growing on and weakly bonded to the BP sheets. Fig. 1d shows that the $CsPbBr_3$ NCs grow on the BP surface with good uniformity and nearly complete coverage. The magnified TEM image (Fig. 1e) clearly shows that perovskite $CsPbBr_3$ NCs are bonded to the BP sheets. The HR-TEM image of the hybrid materials (Fig. 1f) shows that the lattice spacings of $CsPbBr_3$ (0.29 nm) and BP (0.25 nm) are consistent with the typical lattice spacings of $CsPbBr_3$ QDs and BP sheets,

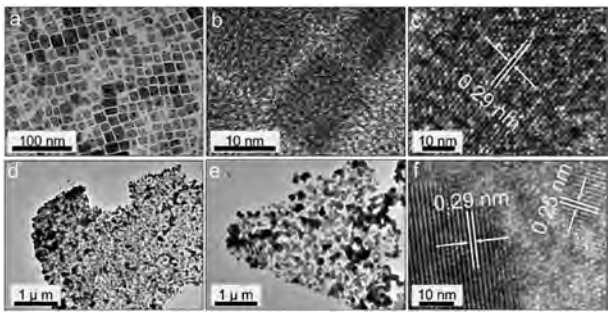

Fig. 1 (a–c) TEM and HR-TEM images of $CsPbBr_3$ QDs synthesized without participation of BP sheets; (d–f) TEM and HR-TEM images of the $CsPbBr_3$–BP hybrid.

revealing that both the $CsPbBr_3$ NCs and the BP sheets in the hybrid structure show good crystallinity. As shown in the large-scale SEM images (Fig. S4, ESI†), all the BP sheets are effectively incorporated with $CsPbBr_3$ NCs with similar uniformity and coverage, implying good adaptability of this strategy in the preparation of $CsPbBr_3$–BP hybrids. The optical microscopy image and fluorescence image of the $CsPbBr_3$–BP hybrid are displayed in Fig. S5a (ESI†), which further confirm the uniform distribution of perovskite NCs on the BP sheets. Notably, as can be seen from the SEM images in the ESI,† the size of the $CsPbBr_3$ NCs in the hybrid structure tends to be in the range of 100 nm. The increase in particle size is probably because the Cs-oleic and Pb-oleic precursors tend to aggregate on the BP surfaces, leading to an accelerated growth of the $CsPbBr_3$ NCs after the initial nucleation.

In this hybrid structure, the distribution density of perovskite NCs on the BP sheets can be controlled by adjusting the quantities of Cs-oleic and Pb-oleic precursors. As shown in Fig. 2, by adding more perovskite precursors, more $CsPbBr_3$ NCs are formed on the BP surface. Furthermore, this hybrid structure also promises controllable broadband response upon simply altering the composition of different halides in perovskite compounds. We demonstrate the feasibility of broadband control by substituting the halide elements, *e.g.*, from bromine to iodine. Fig. S5b (ESI†) shows that the BP sheets with a uniform distribution of $CsPbI_3$ NCs yield fluorescence emission at longer wavelengths. All in all, this fabrication method is compatible with different cesium-containing perovskite materials. The broadband tunability can be achieved by altering the halide composition.[20]

The combination of perovskite NCs with BP can potentially facilitate energy transfer because the perovskite exhibits a stable emission peak that overlaps with BP absorption features. The UV-vis-NIR absorptions of the BP sheets and the $CsPbBr_3$–BP hybrid materials are displayed in Fig. 3a. In contrast to BP sheets, the hybrid materials show an additional band edge absorption at 505 nm,[29] implying that perovskite NCs are combined with BP sheets. In addition, enhanced light absorption can also be observed, demonstrating the ability of perovskite NCs to increase the light absorption of the perovskite–BP hybrid structure. Fig. 3b shows the PL emission of the $CsPbBr_3$–BP hybrid materials. A single narrow emission peak at 510 nm can be observed. The PL decay characteristics of the $CsPbBr_3$ NCs off (the SEM image is shown in Fig. S6, ESI†) and on BP sheets are compared using hybrid samples without centrifugation. The samples are deposited on fused quartz substrates for measurement of the lifetimes. Fig. 3c shows that the PL lifetime is reduced when $CsPbBr_3$ NCs are incorporated within the BP sheets. The PL decay curves fitted with a bi-exponential function[30] show average lifetimes of 1.021 ns and 0.234 ns for $CsPbBr_3$ NCs off and on the BP sheets, respectively. A statistical analysis of the PL average lifetime from a large number of $CsPbBr_3$ NCs is presented in Fig. 3d. $CsPbBr_3$ NCs off the BP sheets exhibit a longer PL lifetime with a peak at 1.05 ns, comparable with previous studies.[29] In contrast, $CsPbBr_3$ NCs prepared *in situ* on BP sheets have shorter PL lifetimes, with a peak at 0.46 ns. Therefore, the PL lifetime of perovskite NCs on BP sheets decreases, suggesting that fluorescence quenching occurs at the interface between the $CsPbBr_3$ NCs and the BP sheets.

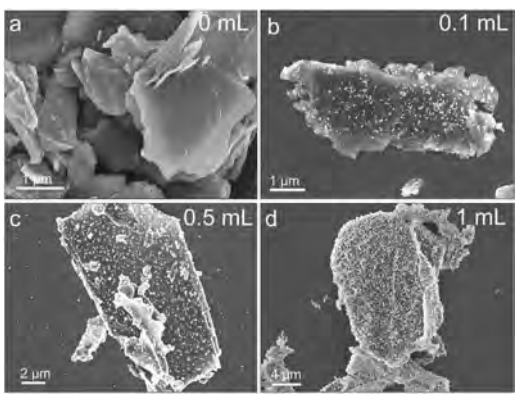

Fig. 2 SEM images of the $CsPbBr_3$–BP hybrid materials synthesized with different amounts of perovskite precursors (a) 0 mL; (b) 0.1 mL; (c) 0.5 mL; (d) 1 mL.

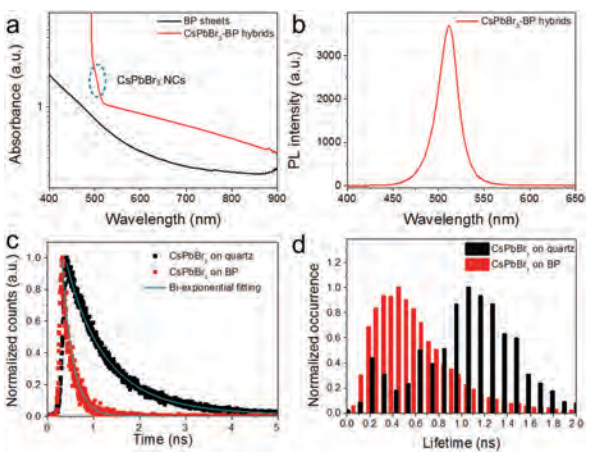

Fig. 3 (a) Absorption spectra of the BP sheets and $CsPbBr_3$–BP hybrids dispersed in a chloroform solution. (b) Corresponding PL spectra of the $CsPbBr_3$–BP hybrid solution irradiated with UV light (365 nm). (c) PL decay curves of $CsPbBr_3$ NCs on fused quartz and BP sheets with the green lines being the fitted results based on a bi-exponential function. (d) Statistical distribution of the lifetimes of $CsPbBr_3$ NCs on fused quartz and BP sheets.

Furthermore, the stability of the $CsPbBr_3$–BP hybrids was evaluated. After being stored for 3 months under ambient conditions, the fluorescence images and Raman scattering spectra of the $CsPbBr_3$–BP hybrid dispersed in chloroform were characterized. The fluorescence images (Fig. S7, ESI†) show that a strong green fluorescence is sustained in the $CsPbBr_3$–BP hybrid. In addition, compared to the freshly-prepared $CsPbBr_3$–BP hybrid, the Raman spectra show that the characteristic A_g^1, B_{2g} and A_g^2 phonon modes of BP are still preserved without significant shift after 3 months, indicating a robust month-long air-stability of the $CsPbBr_3$–BP hybrid.

In summary, a facile solution-based method is designed to prepare perovskite NCs on BP sheets *in situ*. A perovskite–BP heterojunction with strong bonding has been obtained with excellent optical and electronic tunability. Reduced PL lifetimes are observed from perovskite $CsPbBr_3$ NCs on BP sheets, probably due to the non-radiative energy transfer or electron transfer at the perovskite–BP interface. The perovskite–BP hybrid offers a new material system for both a fundamental study and technical design of high-performance optoelectronic devices.

This work was jointly supported by the National Natural Science Foundation of China No. 51672305, Guangdong Province Public Interest Research and Capacity Building Special Fund No. 2017A020216020, Frontier Science Key Programs of Chinese Academy of Sciences No. QYZDB-SSW-SLH034, Science and Technology Key Project of Shenzhen No. JCYJ20140417113430608, City University of Hong Kong Strategic Research Grant (SRG) No. 7004644 and RGC Competitive Earmarked Research Grants, No. 402812 and 14304314. The authors thank Andrew S. K. Li for his valuable technical advice and help in FLIM measurements.

Conflicts of interest

There are no conflicts to declare.

Notes and references

1 D. Kufer and G. Konstantatos, *ACS Photonics*, 2016, **3**, 2197–2210.
2 G. Konstantatos, M. Badioli, L. Gaudreau, J. Osmond, M. Bernechea, F. P. G. de Arquer, F. Gatti and F. H. L. Koppens, *Nat. Nanotechnol.*, 2012, **7**, 363–368.
3 D. Zhang, L. Gan, Y. Cao, Q. Wang, L. Qi and X. Guo, *Adv. Mater.*, 2012, **24**, 2715–2720.
4 F. Federspiel, G. Froehlicher, M. Nasilowski, S. Pedetti, A. Mahmood, B. Doudin, S. Park, J.-O. Lee, D. Halley, B. Dubertret, P. Gilliot and S. Berciaud, *Nano Lett.*, 2015, **15**, 1252–1258.
5 K. Zhang, Y. Wang, W. Jin, X. Fang, Y. Wan, Y. Zhang, J. Han and L. Dai, *RSC Adv.*, 2016, **6**, 25123–25127.
6 M. Gong, Q. Liu, B. Cook, B. Kattel, T. Wang, W.-L. Chan, D. Ewing, M. Casper, A. Strame and J. Z. Wu, *ACS Nano*, 2017, **11**, 4114–4123.
7 D. Kufer, I. Nikitskiy, T. Lasanta, G. Navickaite, F. H. L. Koppens and G. Konstantatos, *Adv. Mater.*, 2015, **27**, 176–180.
8 F. Prins, A. J. Goodman and W. A. Tisdale, *Nano Lett.*, 2014, **14**, 6087–6091.
9 C. Hu, D. Dong, X. Yang, K. Qiao, D. Yang, H. Deng, S. Yuan, J. Khan, Y. Lan, H. Song and J. Tang, *Adv. Funct. Mater.*, 2017, **27**, 1603605.
10 Y. Yu, Y. Zhang, X. Song, H. Zhang, M. Cao, Y. Che, H. Dai, J. Yang, H. Zhang and J. Yao, *ACS Photonics*, 2017, **4**, 950–956.
11 H. Zang, P. K. Routh, Y. Huang, J.-S. Chen, E. Sutter, P. Sutter and M. Cotlet, *ACS Nano*, 2016, **10**, 4790–4796.
12 K. M. Goodfellow, C. Chakraborty, K. Sowers, P. Waduge, M. Wanunu, T. Krauss, K. Driscoll and A. N. Vamivakas, *Appl. Phys. Lett.*, 2016, **108**, 021101.
13 A. Raja, A. M. Castillo, J. Zultak, X.-X. Zhang, Z. Ye, C. Roquelet, D. A. Chenet, A. M. van der Zande, P. Huang, S. Jockusch, J. Hone, D. R. Reichman, L. E. Brus and T. F. Heinz, *Nano Lett.*, 2016, **16**, 2328–2333.
14 A. Boulesbaa, K. Wang, M. M. Samani, M. Tian, A. A. Puretzky, I. Ivanov, C. M. Rouleau, K. Xiao, B. G. Sumpter and D. B. Geohegan, *J. Am. Chem. Soc.*, 2016, **138**, 14713–14719.
15 Y.-F. Xu, M.-Z. Yang, B.-X. Chen, X.-D. Wang, H.-Y. Chen, D.-B. Kuang and C.-Y. Su, *J. Am. Chem. Soc.*, 2017, **139**, 5660–5663.
16 J. Schornbaum, B. Winter, S. P. Schiessl, F. Gannott, G. Katsukis, D. M. Guldi, E. Spiecker and J. Zaumseil, *Adv. Funct. Mater.*, 2014, **24**, 5798–5806.
17 L. Li, Y. Yu, G. J. Ye, Q. Ge, X. Ou, H. Wu, D. Feng, X. H. Chen and Y. Zhang, *Nat. Nanotechnol.*, 2014, **9**, 372–377.
18 X. Ling, H. Wang, S. Huang, F. Xia, M. S. Dresselhaus and J. Lau, *Proc. Natl. Acad. Sci. U. S. A.*, 2015, **112**, 4523–4530.
19 J. Ran, X. Wang, B. Zhu and S.-Z. Qiao, *Chem. Commun.*, 2017, **53**, 9882–9885.
20 F. Liu, Y. Zhang, C. Ding, S. Kobayashi, T. Izuishi, N. Nakazawa, T. Toyoda, T. Ohta, S. Hayase, T. Minemoto, K. Yoshino, S. Dai and Q. Shen, *ACS Nano*, 2017, **11**, 10373–10383.
21 L. Protesescu, S. Yakunin, M. I. Bodnarchuk, F. Krieg, R. Caputo, C. H. Hendon, R. X. Yang, A. Walsh and M. V. Kovalenko, *Nano Lett.*, 2015, **15**, 3692–3696.
22 Y. Zhang, J. Liu, Z. Wang, Y. Xue, Q. Ou, L. Polavarapu, J. Zheng, X. Qi and Q. Bao, *Chem. Commun.*, 2016, **52**, 13637–13655.
23 J. You, Z. Hong, Y. (M.) Yang, Q. Chen, M. Cai, T.-B. Song, C.-C. Chen, S. Lu, Y. Liu, H. Zhou and Y. Yang, *ACS Nano*, 2014, **8**, 1674–1680.
24 Q.-D. Yang, J. Li, Y. Cheng, H.-W. Li, Z. Guan, B. Yu and S.-W. Tsang, *J. Mater. Chem. A*, 2017, **5**, 9852–9858.
25 S. Wei, Y. Yang, X. Kang, L. Wang, L. Huang and D. Pan, *Chem. Commun.*, 2016, **52**, 7265–7268.
26 H. Huang, Q. Xiao, J. Wang, X.-F. Yu, H. Wang, H. Zhang and P. K. Chu, *npj 2D Mater. Appl.*, 2017, **1**, 20.
27 R. Hultgren, N. S. Gingrich and B. E. Warren, *J. Chem. Phys.*, 1935, **3**, 351–355.
28 Z. Guo, S. Chen, Z. Wang, Z. Yang, F. Liu, Y. Xu, J. Wang, Y. Yi, H. Zhang, L. Liao, P. K. Chu and X. F. Yu, *Adv. Mater.*, 2017, **29**, 1703811.
29 M. Pelton, M. I. Bodnarchuk, M. V. Kovalenko and E. Waks, *Appl. Phys. Lett.*, 2017, **111**, 221104.
30 X. Du, G. Wu, J. Cheng, H. Dang, K. Ma, Y.-W. Zhang, P.-F. Tan and S. Chen, *RSC Adv.*, 2017, **7**, 10391–10396.

Electronic Supplementary Information for

In Situ Growth of All-Inorganic Perovskite Nanocrystals on Black Phosphorus Nanosheets

Hao Huang,[a] Jia Li,*[a] Ya Yi,[a] Jiahong Wang,[a] Yihong Kang,[a] Paul K. Chu,[b] H. C. Ong,[c] and Xue-Feng Yu*[a]

[a]Center for Biomedical Materials and Interfaces, Shenzhen Institutes of Advanced Technology, Chinese Academy of Sciences, Shenzhen 518055, China.

[b]Department of Physics and Department of Materials Science and Engineering, City University of Hong Kong, Tat Chee Avenue, Kowloon, Hong Kong, China.

[C]Department of Physics, The Chinese University of Hong Kong, Shatin, Hong Kong, China.

*E-mail address: jia.li1@siat.ac.cn; xf.yu@siat.ac.cn

Experimental details

Materials

The bulk BP crystals were purchased from MoPhos Technology Co. Ltd. (China). Chloroform ($CHCl_3$) was purchased from Shanghai Lingfeng Chemical Reagent Co. Ltd. (Shanghai, China), Cs_2CO_3 (99.99%), PbO (99.9%), (OA) and tetrabutylammonium bromide (TBAB, 99.0%) were obtained from Aladdin Ltd. (Shanghai, China).

Preparation of micrometer-scale BP sheets

The BP sheets were prepared by a modified liquid exfoliation method according to our previous work.[1] In brief, 20 mg of bulk BP crystal was ground in a mortar with 2 mL of chloroform ($CHCl_3$) for 10 min in a glovebox (Argon). The mixture was then added to 18 mL of $CHCl_3$ in a 50 mL glass tube. The tube and sonicator tip were firmly sealed with Teflon tapes. The sample was ultrasonically treated for 3 h at a power of 720 W. Afterwards, the solution was centrifuged for 5 min at 300 rpm and the supernatant containing micrometer-scale BP sheets was collected.

Synthesis of Cs-oleic and Pb-oleic precursor

The Cs-oleic and Pb-oleic precursor was prepared according to the process reported previously.[2] 0.1629 g (0.5 mmol) of Cs_2CO_3 and 0.2232 g (1 mmol) of PbO were mixed with 5 mL of oleic acid (OA) in a 20 mL glass vial. The mixture was placed on a hot plate at 160 °C and stirred vigorously until a transparent solution was formed. Afterwards, the solution was diluted to 10 mL by adding 5 mL of $CHCl_3$.

Synthesis of $CsPbBr_3$ quantum dots and $CsPbBr_3$-BP hybrid

The Br precursor solution was prepared by mixing 0.0644 g (0.2 mmol) of tetrabutylammonium bromide (TBAB), 1 mL of OA, and 4 mL of $CHCl_3$. In the synthesis of $CsPbBr_3$ quantum dots, 1 mL of the Cs and Pb precursor was further diluted with 15 mL of $CHCl_3$ and 2.5 mL of the Br precursor were added quickly to the diluted solution under vigorously stirring for 10 s. The solution turned transparent green and the $CsPbBr_3$ quantum dots were synthesized. In the synthesis of the **$CsPbBr_3$-BP** hybrid, 1 mL of the Cs and Pb precursor was mixed with 7.5 mL of BP sheets (in $CHCl_3$) and 7.5 mL of $CHCl_3$. The mixture was stirred for 5 min. Then 2.5 mL of the Br precursor were added quickly under vigorous stirring for 10 s. The solution became yellow-green and the **$CsPbBr_3$-BP** hybrid were synthesized.

Characterization

The TEM and HR-TEM images were obtained on the FEI Tecnai G2 F30 transmission electron microscope at an acceleration voltage of 200 kV and the SEM images were acquired from the ZEISS SUPRA 55 (Carl Zeiss, Germany) field-emission scanning electron microscope. The UV–vis–NIR absorption spectra were recorded on a Lambda25 spectrophotometer (PerkinElmer) using QS-grade quartz cuvettes at room temperature. The PL spectra were acquired on a fluorescence spectrophotometer (Hitachi F-4600, Japan) and the fluorescence images were recorded on the Olympus-BX63 fluorescence microscope. For the atomic force microscope (AFM) measurement, the as-prepared BP sheets were drop casted on a Si/SiO_2 substrate and dried at 37 °C. The AFM measurement was performed on the Bruker Dimension Icon atomic force microscope (Bruker Corporation, USA) using the tapping mode. The PL lifetime was measured on the Leica SP5 confocal microscopy FLIM (fluorescence lifetime imaging microscopy) system with a 100 × air objective lens (NA = 0.95). A femtosecond pulsed laser with a wavelength of 408nm was used in PL excitation. Photon detection was conducted on

an avalanche photodiode and a synchronous time-correlated single photon counting (TCSPC) module. A high-resolution FLIM areas of ~6 μm^2 containing sufficient $CsPbBr_3$ NCs off and on BP sheets were used to perform the statistical analysis for the PL lifetime. The measured PL decay curves were fitted with a bi-exponential function of time (t):

$$I(t) = A_1 \exp\left(-\frac{t}{\tau_1}\right) + A_2 exp\left(-\frac{t}{\tau_2}\right)$$

Where τ_i represents the decay time of ith component and A_i is the amplitude of the *ith* component. The average lifetime τ_{ave} was estimated from the fitted data according to the equation:

$$\tau_{ave} = \frac{\sum A_i \tau_i^2}{\sum A_i \tau_i}$$

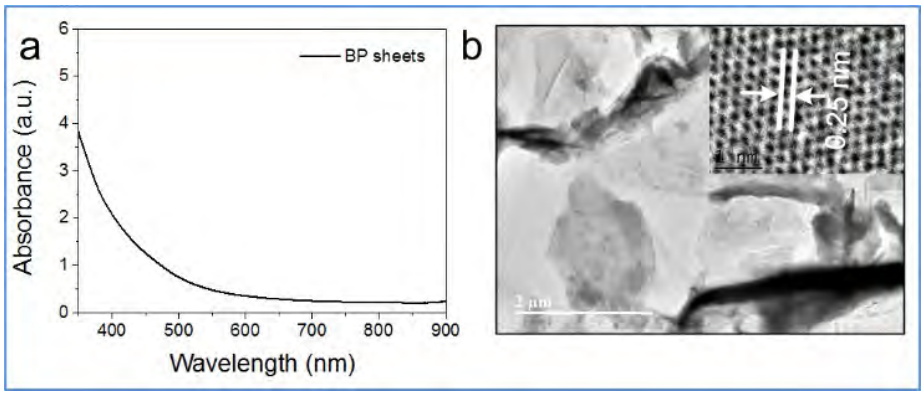

Fig. S1 a) Absorption spectrum of the synthesized BP sheets; b) TEM image and HR-TEM image (inset) of the BP sheets.

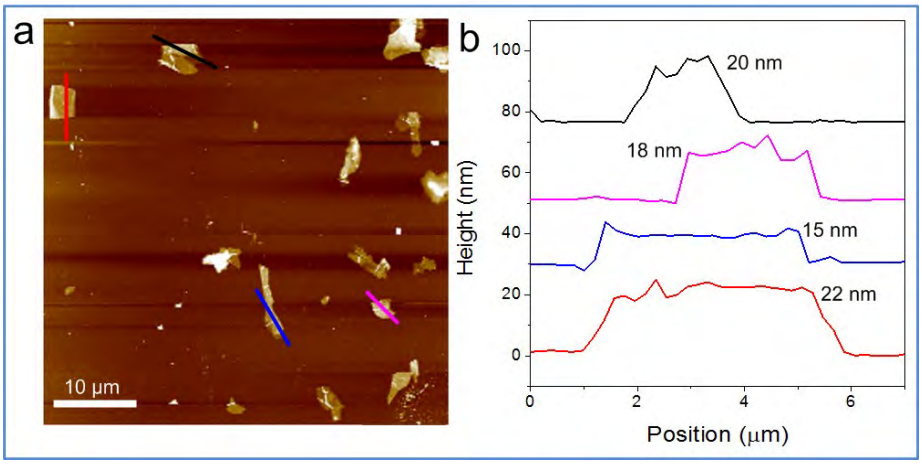

Fig. S2 a) AFM image of as-prepared BP sheets; b) Corresponding height profile of BP sheets

highlighted in a.

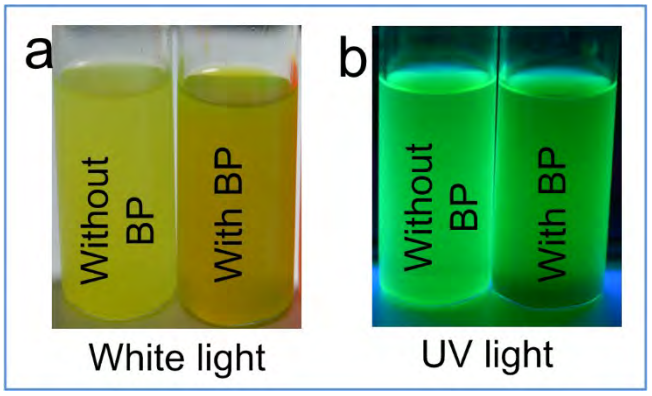

Fig. S3 a) White light and b) UV light images of $CsPbBr_3$ NCs prepared with and without participation of BP sheets.

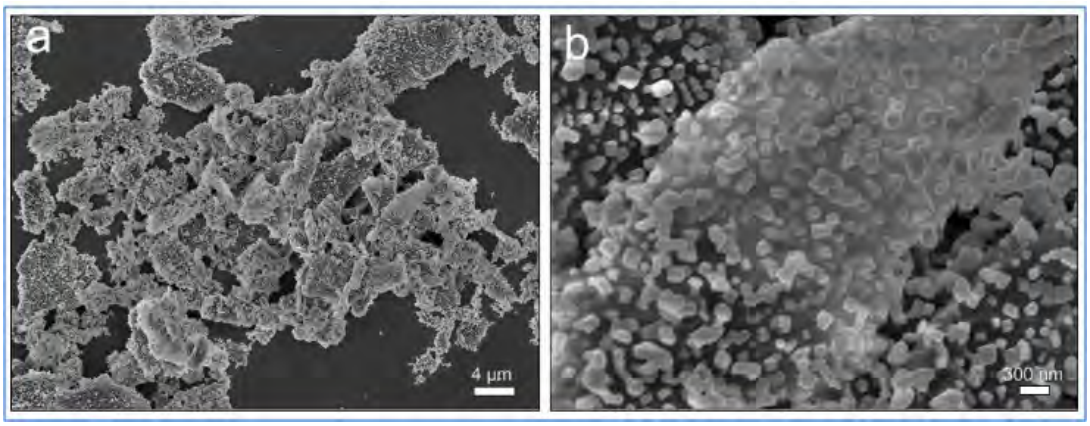

Fig. S4 a) Large scale SEM image of the $CsPbBr_3$-BP hybrid; b) Magnified SEM image of one $CsPbBr_3$-BP hybrid.

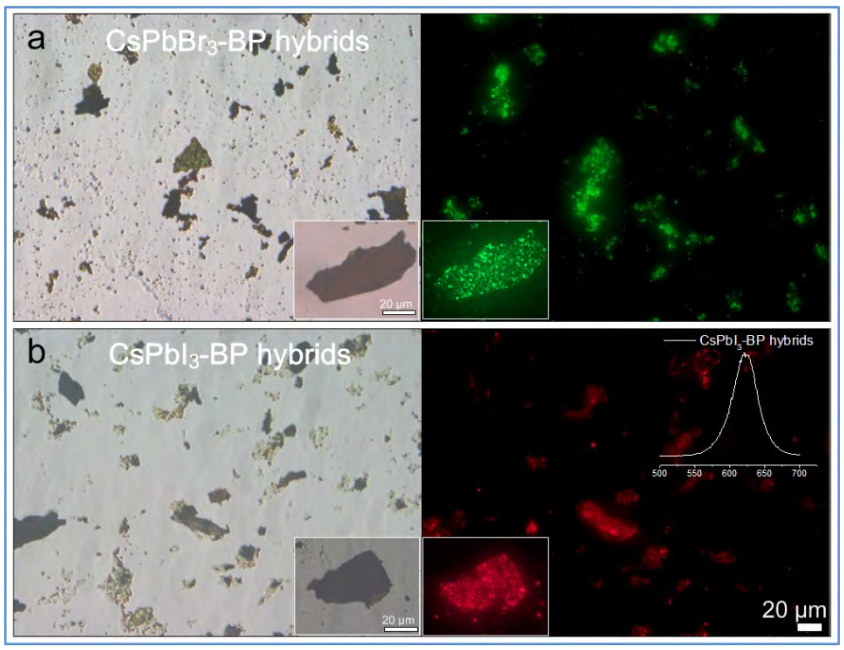

Fig. S5 a) Optical microscopy and PL images of $CsPbBr_3$-BP hybrid with single $CsPbBr_3$-BP hybrid inset; b) Optical microscopy and PL images of $CsPbI_3$-BP hybrid with single $CsPbI_3$-BP hybrid and PL spectrum inset.

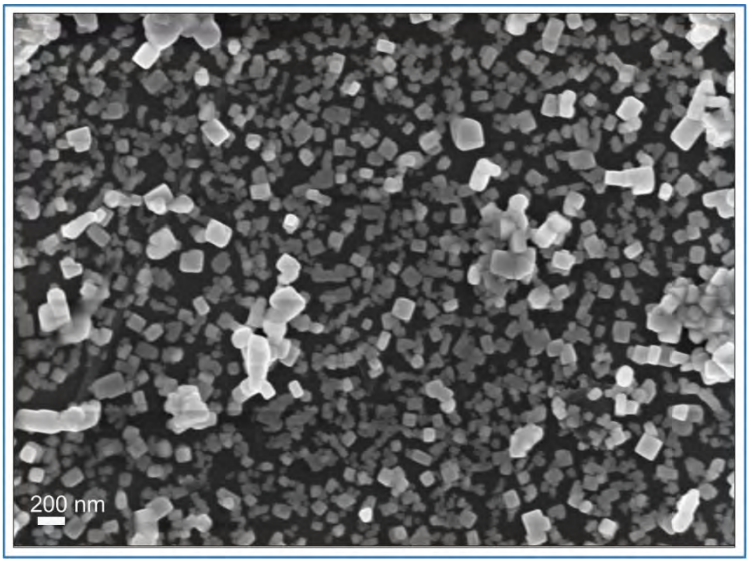

Fig. S6 SEM image of $CsPbBr_3$ NCs off the BP sheets.

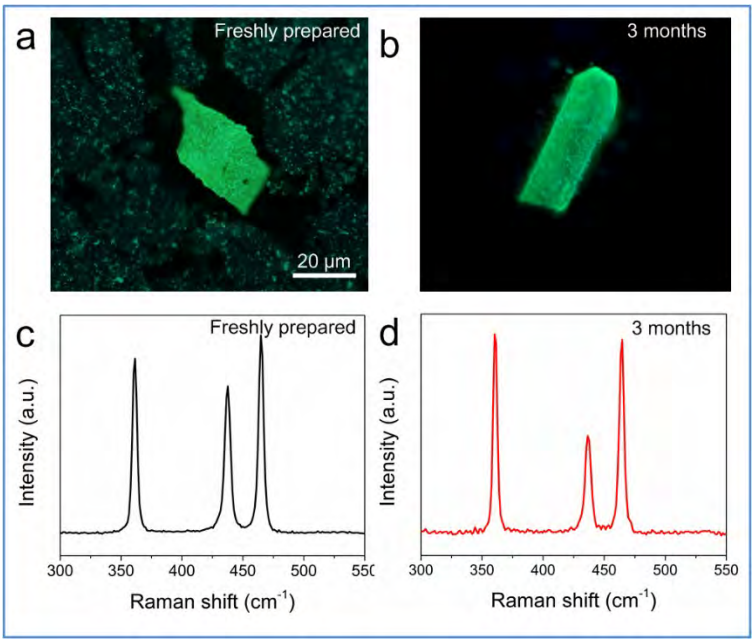

Fig. S7. Fluorescence images of $CsPbBr_3$-BP hybrid which are a) freshly prepared and b) stored under ambient condition for 3 months; Raman spectra of $CsPbBr_3$-BP hybrid which are c) freshly prepared and d) stored under ambient condition for 3 months.

References

1 H. Huang, Q. Xiao, J. Wang, X.-F. Yu, H. Wang, H. Zhang and P. K. Chu, *npj 2D Mater. Appl.,* 2017, **1**, 20.

2 S. Wei, Y. Yang, X. Kang, L. Wang, L. Huang and D. Pan,. *Chem. Commun.*, 2016, **52**, 7265-7268.